IEEE Access
Multidisciplinary | Rapid Review | Open Access Journal

Date of publication xxxx 00, 0000, date of current version xxxx 00, 0000.

Digital Object Identifier 10.1109/ACCESS.2022.Doi Number

Passive Control for Brushless Doubly-Fed Reluctance Generator under Unbalanced Grid Voltages

Xiaoliang Yang[1], Yixuan Qin[1], Jiajun Bai[2], Jihao Zhan[1], Yihao Li[1] and Suya Hao[1]

[1]School of Electrical and Information Engineering, Zhengzhou University of Light Industry, Zhengzhou, China
[2]State Grid Xin Yuan Company Limited, Zhengzhou, China

Corresponding author: Xiaoliang Yang (e-mail: yangxl@hnu.edu.cn).

ABSTRACT To tackle issues like unbalanced currents in stator windings and power pulsations under unbalanced grid voltage conditions, this paper introduces a passive control strategy for the Brushless Doubly-Fed Reluctance Generator (BDFRG). The approach effectively suppresses current distortions in the stator windings, as well as second harmonic pulsations in the active and reactive power. First, the positive and negative sequence equations of the BDFRG are established using the symmetric component method. Then, passive feedback controllers are designed for both positive and negative sequences by using the Euler-Lagrange (EL) model and the passivity theory. Finally, the given values of the positive and negative currents of the power winding and control winding are calculated to obtain the passive feedback controllers for the BDFRG under unbalanced grid voltages. Simulations and hardware in the loop (HIL) experiments are conducted to validate the correctness of the derived model and assess the effectiveness of the control strategy.

INDEX TERMS brushless doubly-fed reluctance generator, passive control strategy, second harmonic pulsations, unbalanced grid voltages

I. INTRODUCTION

The Brushless Doubly-Fed Generator (BDFG) is a novel type of Alternating Current (AC) induction machine in the field of wind power generation [1]-[3]. Its stator comprises two sets of independent windings, namely the Power Winding (PW) and the Control Winding (CW). The PW is linked directly to the grid, whereas the CW is linked to the grid through a converter to regulate the operating speed [4], [5]. The rotor structure determines the operation of the BDFG and the coupling between the PW and CW [6]. The Brushless Doubly-Fed Reluctance Generator (BDFRG) uses salient-pole reluctance instead of short-circuited coils to impede the alternating magnetic flux. Due to the absence of rotor circuits, its robustness, reliability, simplicity, and efficiency are significantly improved [7]-[9]. Reference [10] proposes that BDFRG can achieve high efficiency and constant power output over a wide speed range. It has significant application potential in both independent power systems and grid-tied systems [11], [12]. The Variable Speed Constant Frequency (VSCF) wind power generation system featuring BDFRG is illustrated in Fig. 1.

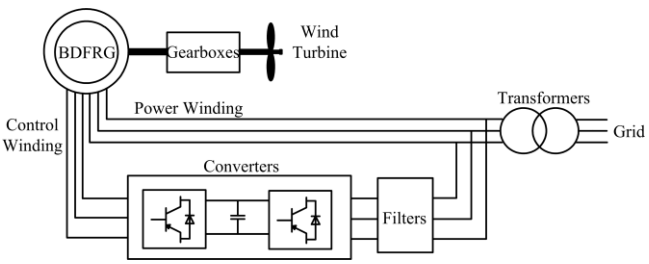

FIGURE 1. VSCF wind power generation system with BDFRG

Several scholars have proposed appropriate control strategies for researching the control of the BDFRG under unbalanced grid voltage conditions. Reference [13] establishes a model of BDFRG under unbalanced grid voltages and analyzes different operational states of balanced and unbalanced grids under low harmonic voltages. Then, it derives equations of positive and negative sequence and provides the theoretical basis of the control method. In response to the challenges faced by wind turbines in achieving decoupled control and dealing with complex control structures under unbalanced grid voltages, the [14] combines Machine

This work was supported in part by the Henan Provincial Science and Technology Research Project under Grant No. 212102210024, the National Natural Science Foundation of China General Program under Grant No. 62273313, Hunan Provincial Natural Science Foundation under Grant No. 2023JJ60178, Graduate Education Reform Project of Henan Province under Grant No.2023SJGLX036Y，2023SJGLX037Y.

Side Converter (MSC) and Grid Side Converter (GSC) to propose a coordinated control strategy. In addressing the problem of distorted currents and voltages of PW side from nonlinear loads, the [15] proposes a control strategy for the independent doubly-fed electric system to eliminate harmonic currents and voltages. In response to the unbalanced currents and voltages of PW side caused by unbalanced loads, the [16] proposes a reactive power loop to generates compensating voltages of the CW side through the MSC. The approach mitigates the CW side overvoltage and eliminates the magnetic flux oscillations of the PW side. To address the 2nd oscillations existing in the output power of generators under unbalanced grid voltages, the [17] proposes a novel control strategy that combines the integral sliding mode and PI controllers. The approach achieves direct power control (DPC) of the generator under unbalanced grid voltages while suppressing the second harmonic fluctuations component in the power.

In [18], an improved vector control strategy for BDFG under unbalanced grid voltages is proposed by introducing a Proportional-Integral-Resonant (PIR) controller. Reference [19] proposes a control method to suppress the harmonic components in the power winding voltage. The control method is to achieve a sinusoidal voltage at the point of common coupling (PCC) by eliminating the 5th and 7th-order voltage components of the PW side. Reference [20] suggests a nonlinear control method for doubly fed wind turbines in positive and negative sequence synchronous rotating coordinate systems based on the passivity theory. By controlling the positive and negative currents of the converters on both sides, the control objectives under unbalanced grid voltages are achieved.

To ensure that wind turbine systems remain grid-connected during voltage dips and to improve their fault ride-through capabilities under such conditions, existing research such as [21] has proposed a current control scheme combining Proportional-Integral (PI) controllers with Resonant (*R*) compensators to precisely control the positive and negative sequence currents of the generator's GSC and RSC. Reference [22] has enhanced the Low Voltage Ride-Through (LVRT) capabilities by incorporating a Demagnetizing Current Controller (DCC) module into traditional crowbar circuits, thus stabilizing the system quickly during transients. Reference [23] addresses the suppression of rotor short-circuit currents with a low-voltage overcurrent control strategy based on tracking, adjusting the rotor flux linkage to follow a smaller proportion of stator flux linkage changes via switching RSC control algorithms. Reference [24] introduces a Forced Demagnetization Controller (FDC) in wind farms, enhancing LVRT capabilities by comparing the effectiveness under three-phase and two-phase faults using the FDC module. Reference [25] utilizes the positive and negative sequences, as well as the natural and forced components in DFIGs, enhancing the modeling capabilities of supercapacitors based on the voltage-capacity relationship to improve the LVRT capabilities of DFIGs against symmetrical and asymmetrical faults.

This paper presents a passive control strategy for BDFRG under unbalanced grid voltages. It effectively suppresses the current distortions in the stator windings, as well as the second harmonic pulsations in the power. Firstly, the positive and negative sequence equations of the BDFRG are constructed using the symmetric component method. Then, based on the Euler-Lagrange (EL) model and passivity theory of the positive and negative sequence BDFRG, passive state feedback controllers for both sequences are designed. Finally, considering the control objectives, the positive and negative sequence reference values of the PW and CW sides currents are calculated to obtain the passive controller for the BDFRG under unbalanced grid voltages. Experimental results on different platforms show that the suggested control strategy can efficiently suppress the current distortions in the PW and CW sides under unbalanced grid voltages, reduce the second harmonic pulsations in the active and reactive power, and enhance the ability to maintain normal operation of the BDFRG under unbalanced grid voltage conditions.

II. THE THEORETICAL MODEL OF BDFRG

A. THE PRINCIPLE OF BDFRG FOR VSCF GENERATION SYSTEM

The BDFRG has two pairs of stator windings, PW and CW. PW is tied directly to the grid, while CW is tied to the grid via a converter. The conversion of mechanical energy into electrical energy is achieved by the modulation of the magnetic flux generated by the current in the stator.

When BDFRG operates with dual stator windings, there is only one type of current on the rotor, resulting in the same angular frequency of induced current in magnetic fields in the rotor with dual stators.

The correlation between the rotor speed, denoted as n_r, and frequency during the operation of BDFRG in a dual-fed mode is as follows:

$$f_p = \frac{n_r(p_p + p_c)}{60} \pm f_c \tag{1}$$

where, n_r is the rotor speed.

Controlling the CW side current frequency as the rotor speed varies enables better maintenance of the stability of the PW side current frequency in the BDFRG. This allows the BDFRG to achieve variable speed constant frequency generation.

B. THE THEORETICAL MODEL UNDER BALANCED GRID

The theoretical model of the BDFRG in the synchronous reference frame of two-phase *d-q* rotation is as follows:

$$\begin{cases} u_{pd} = R_p i_{pd} + p\psi_{pd} - \omega_p \psi_{pq} \\ u_{pq} = R_p i_{pq} + p\psi_{pq} + \omega_p \psi_{pd} \\ u_{cd} = R_c i_{cd} + p\psi_{cd} - \omega_c \psi_{cq} \\ u_{cq} = R_c i_{cq} + p\psi_{cq} + \omega_c \psi_{cd} \\ \omega_p = \omega \\ \omega_c = \omega_r - \omega \end{cases} \tag{2}$$

$$\begin{cases} \psi_{pd} = L_p i_{pd} + L_m i_{cd} \\ \psi_{pq} = L_p i_{pq} - L_m i_{cq} \\ \psi_{cd} = L_c i_{cd} + L_m i_{pd} \\ \psi_{cq} = L_c i_{cq} - L_m i_{pq} \end{cases} \tag{3}$$

where, $p = \mathrm{d}/\mathrm{d}t$ is the differential operator.

The parameters in the theoretical model and their significance are displayed in Table I.

TABLE I
BDFRG PARAMETER AND SIGNIFICANCE

Parameter	Significance
ψ_{pd}, ψ_{pq}, ψ_{cd}, ψ_{cq}	the d and q axis magnetic fluxes of PW and CW
u_{pd}, u_{pq}, u_{cd}, u_{cq}	the d and q axis voltages of PW and CW
i_{pd}, i_{pq}, i_{cd}, i_{cq}	the d and q axis currents of PW and CW
R_p, R_c	resistances of PW and CW
L_p, L_c, L_m	self-inductances of PW and CW, mutual inductance between PW and CW
ω_p, ω_c, ω_r	angular velocities of PW and CW, rotor in arbitrary speed rotating reference frames
p_p, p_c	pole pairs of PW and CW
f_p, f_c	current frequencies of PW and CW

The equivalent schematic diagram of the BDFRG is depicted in Fig. 2.

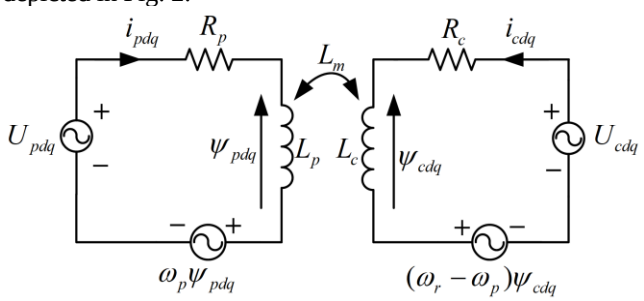

FIGURE 2. Equivalent schematic diagram of the BDFRG

C. THE THEORETICAL MODEL UNDER UNBALANCED GRID

When the BDFRG is operating in unbalanced grid voltages, asymmetric components will be generated compared to its normal operating state.

According to the theory of symmetrical components, each unbalanced three-phase system component in an unbalanced grid can be separated into three balanced three-phase systems components: positive sequence, negative sequence, and zero sequence. The zero sequence can be disregarded as it has no impact on the behavior of BDFRG [26]-[28].

Therefore, when the system voltage is unbalanced, the variables are including positive and negative sequence components. Typically, any unbalanced vector of the PW side in a steady state can be written as:

$$x_p = x_{p+} e^{j(\omega_p t + \theta_{p+})} + x_{p-} e^{j(-\omega_p t + \theta_{p-})} \tag{4}$$

Substituting (4) into the main reference frame, we obtain:

$$x_p = x_{p+} e^{j\theta_{p+}} + x_{p-} e^{j\theta_{p-}} e^{-j2\omega_p t} \tag{5}$$

Equation (5) can also be expressed by rewriting it as:

$$x_p = x_p^+ + x_p^- e^{-j2\omega_p t} \tag{6}$$

where, x_{p+} and x_{p-} are the vector magnitudes of positive and negative sequences. θ_{p+} and θ_{p-} are the initial angular positions of positive and negative sequences. x_p^+ and x_p^- are in their respective positive and negative reference frames with angular frequencies of ω_p and $-\omega_p$.

The frequency of the CW side depends on the frequency of the PW side. The PW side includes two angular frequencies, denoted by ω_p and $-\omega_p$, while the CW side variables include two angular frequencies, denoted by $\omega_r - \omega_p$ and $\omega_r + \omega_p$. Therefore, in an unbalanced grid, any vector of the CW side can be expressed as:

$$x_c = x_{c+} e^{j((\omega_r - \omega_p)t + \theta_{c+})} + x_{c-} e^{j((\omega_r + \omega_p)t + \theta_{c-})} \tag{7}$$

Substituting (7) into the main reference frame, we obtain:

$$x_c = x_{c+} e^{j\theta_{c+}} + x_{c-} e^{j\theta_{c-}} e^{j2\omega_p t} \tag{8}$$

Equation (8) can also be expressed by rewriting it as:

$$x_c = x_c^+ + x_c^- e^{j2\omega_p t} \tag{9}$$

where, x_{c+} and x_{c-} are the vector magnitudes of positive and negative sequences, while θ_{c+} and θ_{c-} are the initial angular positions of positive and negative sequences. x_c^+ and x_c^- are in their respective positive and negative reference frames with angular frequencies of $\omega_r - \omega_p$ and $\omega_r + \omega_p$.

The vector graph of the stator magnetic flux orientation under unbalanced grid voltages is depicted in Fig. 3.

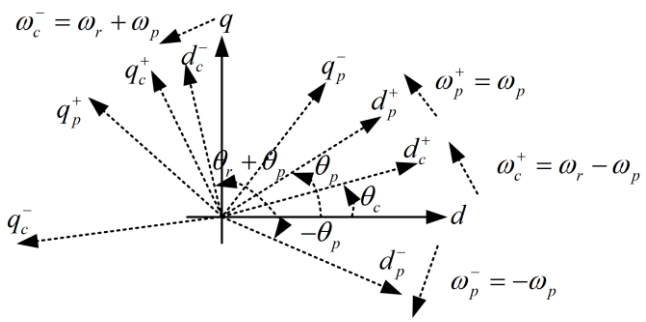

FIGURE 3. Vector graph of the stator magnetic flux orientation under unbalanced grid voltages

By substituting (2) and (3) into (6) and (9), and then expanding and rearranging, we can obtain the positive sequence equations of the stator magnetic flux and voltage of the BDFRG under unbalanced grid voltages.

$$\begin{cases} u_{pd}^{+} = R_p i_{pd}^{+} + p\psi_{pd}^{+} - \omega_p^{+}\psi_{pq}^{+} \\ u_{pq}^{+} = R_p i_{pq}^{+} + p\psi_{pq}^{+} + \omega_p^{+}\psi_{pd}^{+} \\ u_{cd}^{+} = R_c i_{cd}^{+} + p\psi_{cd}^{+} - (\omega_r - \omega_p^{+})\psi_{cq}^{+} \\ u_{cq}^{+} = R_c i_{cq}^{+} + p\psi_{cq}^{+} + (\omega_r - \omega_p^{+})\psi_{cd}^{+} \end{cases} \tag{10}$$

$$\begin{cases} \psi_{pd}^{+} = L_p i_{pd}^{+} + L_m i_{cd}^{+} \\ \psi_{pq}^{+} = L_p i_{pq}^{+} - L_m i_{cq}^{+} \\ \psi_{cd}^{+} = L_c i_{cd}^{+} + L_m i_{pd}^{+} \\ \psi_{cq}^{+} = L_c i_{cq}^{+} - L_m i_{pq}^{+} \end{cases} \tag{11}$$

where, u_{pd}^{+} and u_{pq}^{+} are the positive voltages along the *d* and *q* axes, in the stator PW's positive sequence *d*-*q* rotating coordinate system. i_{pd}^{+} and i_{pq}^{+} are the positive currents along the *d* and *q* axes, in the stator PW's positive sequence *d*-*q* rotating coordinate system. u_{cd}^{+} and u_{cq}^{+} are the positive voltages along the *d* and *q* axes, in the stator CW's positive sequence *d*-*q* rotating coordinate system. i_{cd}^{+} and i_{cq}^{+} are the positive currents along the *d* and *q* axes, in the stator CW's positive sequence *d*-*q* rotating coordinate system. ψ_{pd}^{+} and ψ_{pq}^{+} are the positive magnetic fluxes along the *d* and *q* axes, in the stator PW's positive sequence *d*-*q* rotating coordinate system. ψ_{cd}^{+} and ψ_{cq}^{+} are the positive magnetic fluxes along the *d* and *q* axes, in the stator CW's positive sequence *d*-*q* rotating coordinate system. $\omega_p^{+} = \omega_p$ and $\omega_c^{+} = \omega_r - \omega_p$ are the angular velocities in any speed positive sequence rotating reference frame of the PW and CW.

The negative sequence equations of the stator magnetic flux and voltage of the BDFRG under unbalanced grid voltages are as follows:

$$\begin{cases} u_{pd}^{-} = R_p i_{pd}^{-} + p\psi_{pd}^{-} - \omega_p^{-}\psi_{pq}^{-} \\ u_{pq}^{-} = R_p i_{pq}^{-} + p\psi_{pq}^{-} + \omega_p^{-}\psi_{pd}^{-} \\ u_{cd}^{-} = R_c i_{cd}^{-} + p\psi_{cd}^{-} - (\omega_r - \omega_p^{-})\psi_{cq}^{-} \\ u_{cq}^{-} = R_c i_{cq}^{-} + p\psi_{cq}^{-} + (\omega_r - \omega_p^{-})\psi_{cd}^{-} \end{cases} \tag{12}$$

$$\begin{cases} \psi_{pd}^{-} = L_p i_{pd}^{-} + L_m i_{cd}^{-} \\ \psi_{pq}^{-} = L_p i_{pq}^{-} - L_m i_{cq}^{-} \\ \psi_{cd}^{-} = L_c i_{cd}^{-} + L_m i_{pd}^{-} \\ \psi_{cq}^{-} = L_c i_{cq}^{-} - L_m i_{pq}^{-} \end{cases} \tag{13}$$

where, u_{pd}^{-} and u_{pq}^{-} are the negative voltages along the *d* and *q* axes, in the stator PW's negative sequence *d*-*q* rotating coordinate system. i_{pd}^{-} and i_{pq}^{-} are the negative currents along the *d* and *q* axes, in the stator PW's negative sequence *d*-*q* rotating coordinate system. u_{cd}^{-} and u_{cq}^{-} are the negative voltages along the *d* and *q* axes, in the stator CW's negative sequence *d*-*q* rotating coordinate system. i_{cd}^{-} and i_{cq}^{-} are the negative currents along the *d* and *q* axes, in the stator CW's negative sequence *d*-*q* rotating coordinate system. ψ_{pd}^{-} and ψ_{pq}^{-} are the negative magnetic fluxes along the *d* and *q* axes, in the stator PW's negative sequence *d*-*q* rotating coordinate system. ψ_{cd}^{-} and ψ_{cq}^{-} are the negative magnetic fluxes along the *d* and *q* axes, in the stator CW's negative sequence *d*-*q* rotating coordinate system. $\omega_p^{-} = -\omega_p$ and $\omega_c^{-} = \omega_r + \omega_p$ are the angular velocities in any speed negative sequence rotating reference frame of the PW.

In the unbalanced grid voltages, our primary control objective is to manage the output active and reactive power of the PW side.

$$\begin{aligned} P &= \frac{3}{2}\mathrm{Re}\left[U_{pdq}^{+} I_{pdq}^{+*}\right] \\ &= \frac{3}{2}\begin{bmatrix} U_{pd}^{+} i_{pd}^{+} + U_{pq}^{+} i_{pq}^{+} + U_{pd}^{-} i_{pq}^{-} + U_{pq}^{-} i_{pq}^{-} \\ +\cos(2\omega_p t)(U_{pd}^{+} i_{pd}^{-} + U_{pq}^{-} i_{pq}^{+} + U_{pq}^{+} i_{pq}^{-} + U_{pd}^{-} i_{pd}^{+}) \\ +\sin(2\omega_p t)(-U_{pd}^{+} i_{pq}^{-} - U_{pd}^{-} i_{pq}^{+} + U_{pq}^{+} i_{pd}^{-} + U_{pq}^{-} i_{pd}^{+}) \end{bmatrix} \\ &= P_{dc} + P_{\cos} + P_{\sin} \\ &= P_{dc} + P_x \end{aligned} \tag{14}$$

$$\begin{aligned} Q &= \frac{3}{2}\mathrm{Im}\left[U_{pdq}^{+} I_{pdq}^{+*}\right] \\ &= \frac{3}{2}\begin{bmatrix} -U_{pd}^{+} i_{pq}^{+} + U_{pq}^{+} i_{pd}^{+} - U_{pd}^{-} i_{pq}^{-} + U_{pq}^{-} i_{pd}^{-} \\ +\cos(2\omega_p t)(-U_{pd}^{+} i_{pq}^{-} - U_{pd}^{-} i_{pq}^{+} + U_{pq}^{+} i_{pd}^{-} + U_{pq}^{-} i_{pd}^{+}) \\ +\sin(2\omega_p t)(-U_{pd}^{+} i_{pd}^{-} - U_{pd}^{-} i_{pd}^{+} - U_{pq}^{+} i_{pq}^{-} - U_{pq}^{-} i_{pq}^{+}) \end{bmatrix} \\ &= Q_{dc} + Q_{\cos} + Q_{\sin} \\ &= Q_{dc} + Q_x \end{aligned} \tag{15}$$

where, P_{dc} and Q_{dc} are the direct current (DC) components of the active and reactive power. $P_{\sin}$, $P_{\cos}$, $Q_{\sin}$, and $Q_{\cos}$ are the second harmonic sine and cosine pulsations of the active and reactive power. P_x and Q_x are the sum of the second harmonic pulsations of the active and reactive power.

From (14) and (15), it can be deduced that the second harmonic cosine and sine pulsations of the active and reactive power respectively are:

$$\begin{cases} P_{\sin} = -U_{pd}^{+} i_{pq}^{-} - U_{pd}^{-} i_{pq}^{+} + U_{pq}^{+} i_{pd}^{-} + U_{pq}^{-} i_{pd}^{+} \\ P_{\cos} = U_{pd}^{+} i_{pd}^{-} + U_{pq}^{-} i_{pq}^{+} + U_{pq}^{+} i_{pq}^{-} + U_{pd}^{-} i_{pd}^{+} \end{cases} \tag{16}$$

$$\begin{cases} Q_{\sin} = -U_{pd}^{+} i_{pd}^{-} - U_{pd}^{-} i_{pd}^{+} - U_{pq}^{+} i_{pq}^{-} - U_{pq}^{-} i_{pq}^{+} \\ Q_{\cos} = -U_{pd}^{+} i_{pq}^{-} - U_{pd}^{-} i_{pq}^{+} + U_{pq}^{+} i_{pd}^{-} + U_{pq}^{-} i_{pd}^{+} \end{cases} \tag{17}$$

III. PASSIVE CONTROL STRATEGY

A. PASSIVITY ANALYSIS

The positive and negative sequence equations have identical coefficients, so they exhibit identical stability characteristics. Therefore, when conducting a passivity analysis of the system, it is sufficient to analyze the passivity of the positive sequence equations to deduce the passivity of the equations of the negative sequence.

According to the stator flux orientation method in the positive sequence synchronous rotating reference frame, the magnetic flux and voltage components along the d^+ and q^+ axes are denoted by $\psi_{pd}^+ = \psi_p^+$, $\psi_{pq}^+ = 0$, $U_{pq}^+ = U_p^+$, and $U_{pd}^+ = 0$.

Let the positive sequence of the *d*-*q* axes of the PW and CW sides currents be the positive sequence of the state variables of the BDFRG system.

$$x^+ = \begin{bmatrix} i_{pd}^+ & i_{pq}^+ & i_{cd}^+ & i_{cq}^+ \end{bmatrix}^T = \begin{bmatrix} x_1^+ & x_2^+ & x_3^+ & x_4^+ \end{bmatrix}^T \quad (18)$$

Formulate the Euler-Lagrange model for the positive sequence equations of the BDFRG system.

$$\boldsymbol{u}^+ = \boldsymbol{D}\dot{\boldsymbol{x}}^+ + \boldsymbol{J}\boldsymbol{x}^+ + \boldsymbol{R}\boldsymbol{x}^+ + \boldsymbol{W} \quad (19)$$

where, $\boldsymbol{D}$ is a positive definite matrix, and $\boldsymbol{J}$ is an antisymmetric matrix, indicating the energy transfer characteristics of the system. $\boldsymbol{R}$ and $\boldsymbol{W}$ are the dissipative matrices, representing the dissipative characteristics of the system. $\boldsymbol{u}^+ = \begin{bmatrix} U_{pd}^+ & U_{pq}^+ & U_{cd}^+ & U_{cq}^+ \end{bmatrix}^T$ is the input parameter of the system, reflecting the energy transfer between the system and the surrounding environment. $\boldsymbol{x}^+ = \begin{bmatrix} i_{pd}^+ & i_{pq}^+ & i_{cd}^+ & i_{cq}^+ \end{bmatrix}^T$ is the state parameter of the system.

The specific form of each part in the Euler-Lagrange structure is as follows:

$$\boldsymbol{D} = \begin{bmatrix} L_p & 0 & L_m & 0 \\ 0 & L_p & 0 & L_m \\ L_m & 0 & L_c & 0 \\ 0 & L_m & 0 & L_c \end{bmatrix} \quad (20)$$

$$\boldsymbol{J} = \begin{bmatrix} 0 & -\omega_c^+ L_p & 0 & -\omega_c^+ L_m \\ \omega_c^+ L_p & 0 & \omega_c^+ L_m & 0 \\ 0 & -\omega_c^+ L_m & 0 & -\omega_c^+ L_c \\ \omega_c^+ L_m & 0 & \omega_c^+ L_c & 0 \end{bmatrix} \quad (21)$$

$$\boldsymbol{R} = \begin{bmatrix} R_p & 0 & 0 & 0 \\ 0 & R_p & 0 & 0 \\ 0 & 0 & R_c & 0 \\ 0 & 0 & 0 & R_c \end{bmatrix} \quad (22)$$

$$\boldsymbol{W} = \begin{bmatrix} 2\omega_c^+ L_m i_{cq}^+ + \omega_r \psi_{pq}^+ - 2\omega_p^+ \psi_{pq}^+ \\ -\omega_r \psi_{pd}^+ + 2\omega_p^+ \psi_{pd}^+ - 2L_m p i_{cq}^+ \\ 2\omega_c^+ L_m i_{pq}^+ \\ -2L_m p i_{pq}^+ \end{bmatrix} \quad (23)$$

The concept of passivity is defined as follows: For the general system with multiple inputs and multiple outputs, if there exists a positive definite function $Q(\boldsymbol{x})$ and a positive semi-definite and continuously derivable energy storage function $H(\boldsymbol{x})$, then when the dissipative inequality (24) holds, the system is strictly passive.

$$H(\boldsymbol{x}_t^+) - H(\boldsymbol{x}_0^+) \le \int_0^t \boldsymbol{u}^{+T} \boldsymbol{y} \mathrm{d}\tau - \int_0^t Q(\boldsymbol{x}^+) \mathrm{d}\tau \quad (24)$$

The passivity of the system reflects the property of energy change. Let $H(\boldsymbol{x})$ be the energy storage function.

$$H = \frac{1}{2} \boldsymbol{x}^{+T} \boldsymbol{D} \boldsymbol{x}^+ \quad (25)$$

Taking the derivative of (25) with respect to time and substituting it into (19), we obtain:

$$\dot{H} = \boldsymbol{x}^{+T} \boldsymbol{D} \dot{\boldsymbol{x}}^+ = \boldsymbol{x}^{+T} \boldsymbol{u}^+ - \boldsymbol{x}^{+T} \boldsymbol{R} \boldsymbol{x}^+ - \boldsymbol{x}^{+T} \boldsymbol{J} \boldsymbol{x}^+ - \boldsymbol{x}^{+T} \boldsymbol{W} \quad (26)$$

Since $\boldsymbol{J}$ is an antisymmetric matrix, the term involving $\boldsymbol{x}^{+T} \boldsymbol{J} \boldsymbol{x}^+ = 0$ does not influence the system energy balance, nor does it impact the stability of the system. Therefore, it must be eliminated when designing the controller, which simplifies the process of the control strategy for the system.

The integration of the equation with respect to the time from t_0 to t, and since both $\boldsymbol{x}^{+T} \boldsymbol{R} \boldsymbol{x}^+$ and $\boldsymbol{x}^{+T} \boldsymbol{W}$ are positive, we have:

$$\begin{aligned} & H(\boldsymbol{x}_t^+) - H(\boldsymbol{x}_0^+) \\ &= \int_{t_0}^t \boldsymbol{x}^{+T} \boldsymbol{u}^+ \mathrm{d}\tau - \int_{t_0}^t \boldsymbol{x}^{+T} \boldsymbol{R} \boldsymbol{x}^+ \mathrm{d}\tau - \int_{t_0}^t \boldsymbol{x}^{+T} \boldsymbol{W} \mathrm{d}\tau \\ &\le \int_{t_0}^t \boldsymbol{x}^{+T} \boldsymbol{u}^+ \mathrm{d}\tau - \int_{t_0}^t \boldsymbol{x}^{+T} \boldsymbol{R} \boldsymbol{x}^+ \mathrm{d}\tau \end{aligned} \quad (27)$$

The equation above is the energy balance equation. On the right-hand side, the first term indicates the electrical energy supplied to the CW side by the converter, the next term shows the electrical resistant losses consumed by the CW side, and the third term represents the portion of energy converted into mechanical energy by the CW side. On the left-hand side, the increment of energy stored in the CW side is always less than the energy supplied to the CW side. It indicates that the system is strictly passive.

If we consider $\boldsymbol{x}^+ = \begin{bmatrix} i_{pd}^+ & i_{pq}^+ & i_{cd}^+ & i_{cq}^+ \end{bmatrix}^T$ as the input to the system and $\boldsymbol{u}^+ = \begin{bmatrix} U_{pd}^+ & U_{pq}^+ & U_{cd}^+ & U_{cq}^+ \end{bmatrix}^T$ as the output, and the mapping from $\boldsymbol{x}^+$ to the output $\boldsymbol{u}^+$ is strictly passive, then it can be inferred that the positive sequence components system is strictly passive. Therefore, passive control can be employed, and the control system is stable.

Using the above strategy, it is also possible to deduce that mapping from $\boldsymbol{x}^-$ to the output $\boldsymbol{u}^-$ strictly passively results in the negative sequence components system also being strictly passive as well. Consequently, this ensures that under unbalanced grid voltages, the BDFRG operating system remains strictly passive.

B. DESIGN OF PASSIVITY FEEDBACK CONTROLLER

The above analysis shows that the system's passivity is directly related to the defined input-output variables of the BDFRG. An appropriate selection of $\boldsymbol{x}^*$ should be selected to receive both Lyapunov stability and excellent tracking performance. The expected value of the system state is:

$$\boldsymbol{x}^* = \begin{bmatrix} x_1^* & x_2^* & x_3^* & x_4^* \end{bmatrix}^T \tag{28}$$

Let $\boldsymbol{x}_e = \boldsymbol{x} - \boldsymbol{x}^*$ denote the difference between the state steady value and the actual value, we obtain:

$$\boldsymbol{u} = \boldsymbol{D}\dot{\boldsymbol{x}}_e + \boldsymbol{J}\boldsymbol{x}_e + \boldsymbol{R}\boldsymbol{x}_e + \boldsymbol{W} \tag{29}$$

The error dynamic equation is obtained as shown in (30) by combining (19).

$$\boldsymbol{D}\dot{\boldsymbol{x}}_e + \boldsymbol{J}\boldsymbol{x}_e + \boldsymbol{R}\boldsymbol{x}_e = \boldsymbol{u} - [\boldsymbol{D}\dot{\boldsymbol{x}}^* + \boldsymbol{J}\boldsymbol{x}^* + \boldsymbol{R}\boldsymbol{x}^* + \boldsymbol{W}] \tag{30}$$

When the energy storage function of the error dynamic equation tends to zero, the system reaches asymptotic stability. Therefore, we define the energy storage function as:

$$H(\boldsymbol{x}_e) = \frac{1}{2}\boldsymbol{x}_e^T \boldsymbol{D}\boldsymbol{x}_e \tag{31}$$

Taking the derivative of (31) with respect to time as:

$$\begin{aligned} \dot{H}(\boldsymbol{x}_e) &= \boldsymbol{x}_e^T \boldsymbol{D}\dot{\boldsymbol{x}}_e \\ &= \boldsymbol{x}_e^T \left\{ \boldsymbol{u} - \left[\boldsymbol{D}\dot{\boldsymbol{x}}^* + \boldsymbol{J}\boldsymbol{x}^* + \boldsymbol{R}\boldsymbol{x}^* + \boldsymbol{W} \right] - \boldsymbol{J}\boldsymbol{x}_e - \boldsymbol{R}\boldsymbol{x}_e \right\} \\ &= \boldsymbol{x}_e^T \left\{ \boldsymbol{u} - \left[\boldsymbol{D}\dot{\boldsymbol{x}}^* + \boldsymbol{J}\boldsymbol{x}^* + \boldsymbol{R}\boldsymbol{x}^* + \boldsymbol{W} \right] \right\} - \boldsymbol{x}_e^T \boldsymbol{J}\boldsymbol{x}_e - \boldsymbol{x}_e^T \boldsymbol{R}\boldsymbol{x}_e \\ &= \boldsymbol{x}_e^T \left\{ \boldsymbol{u} - \left[\boldsymbol{D}\dot{\boldsymbol{x}}^* + \boldsymbol{J}\boldsymbol{x}^* + \boldsymbol{R}\boldsymbol{x}^* + \boldsymbol{W} \right] \right\} - \boldsymbol{x}_e^T \boldsymbol{R}\boldsymbol{x}_e \end{aligned} \tag{32}$$

In order to ensure that the entire control system is strictly passive and to improve the dynamic response of the system. The function $H(\boldsymbol{x}_e)$ should quickly tend to zero, so we introduce damping injection $\boldsymbol{S}_a = diag(S_{pd}, S_{pq}, S_{cd}, S_{cq})$ as shown in (33).

$$\boldsymbol{u} - \left[\boldsymbol{D}\dot{\boldsymbol{x}}^* + \boldsymbol{J}\boldsymbol{x}^* + \boldsymbol{R}\boldsymbol{x}^* + \boldsymbol{W} \right] = -\boldsymbol{S}_a \boldsymbol{x}_e \tag{33}$$

Substituting (33) into (32), we obtain:

$$\dot{H}(\boldsymbol{x}_e) = -\boldsymbol{x}_e^T (\boldsymbol{R} + \boldsymbol{S}_a)\boldsymbol{x}_e < 0 \tag{34}$$

According to Lyapunov stability, since $\boldsymbol{D}$ is a positive definite matrix, the function $H(\boldsymbol{x}_e) > 0$. Therefore, the control strategy is asymptotically stable. The designed passive control law according to (33) can be expressed as:

$$\boldsymbol{u} = \left[\boldsymbol{D}\dot{\boldsymbol{x}}^* + \boldsymbol{J}\boldsymbol{x}^* + \boldsymbol{R}\boldsymbol{x}^* + \boldsymbol{W} \right] - \boldsymbol{S}_a \boldsymbol{x}_e \tag{35}$$

Since the stator voltages are uncontrollable variables, we set $S_{pd} = S_{pq} = 0$. By expanding (26), we have derived the passive control law for the BDFRG, which is presented in (36).

$$\begin{aligned} \begin{bmatrix} u_{cd} \\ u_{cq} \end{bmatrix} &= \begin{bmatrix} L_m & 0 & L_c & 0 \\ 0 & L_m & 0 & L_c \end{bmatrix} \begin{bmatrix} pi_{pd}^* \\ pi_{pq}^* \\ pi_{cd}^* \\ pi_{cq}^* \end{bmatrix} \\ &+ \begin{bmatrix} R_c & 0 \\ 0 & R_c \end{bmatrix} \begin{bmatrix} i_{cd}^* \\ i_{cq}^* \end{bmatrix} \\ &+ \begin{bmatrix} 0 & -\omega_c L_m & 0 & -\omega_c L_c \\ \omega_c L_m & 0 & \omega_c L_c & 0 \end{bmatrix} \begin{bmatrix} i_{pd}^* \\ i_{pq}^* \\ i_{cd}^* \\ i_{cq}^* \end{bmatrix} \\ &+ \begin{bmatrix} 2\omega_c L_m i_{pq} \\ -2L_m p i_{pq} \end{bmatrix} - \begin{bmatrix} S_{cd}(i_{cd} - i_{cd}^*) \\ S_{cq}(i_{cq} - i_{cq}^*) \end{bmatrix} \end{aligned} \tag{36}$$

Since $\boldsymbol{x}^*$ remain constant, we can simplify (36) to:

$$\begin{aligned} \begin{bmatrix} u_{cd} \\ u_{cq} \end{bmatrix} &= \begin{bmatrix} R_c & 0 \\ 0 & R_c \end{bmatrix} \begin{bmatrix} i_{cd}^* \\ i_{cq}^* \end{bmatrix} \\ &+ \begin{bmatrix} 0 & -\omega_c L_m & 0 & -\omega_c L_c \\ \omega_c L_m & 0 & \omega_c L_c & 0 \end{bmatrix} \begin{bmatrix} i_{pd}^* \\ i_{pq}^* \\ i_{cd}^* \\ i_{cq}^* \end{bmatrix} \\ &+ \begin{bmatrix} 2\omega_c L_m i_{pq} \\ -2L_m p i_{pq} \end{bmatrix} - \begin{bmatrix} S_{cd}(i_{cd} - i_{cd}^*) \\ S_{cq}(i_{cq} - i_{cq}^*) \end{bmatrix} \end{aligned} \tag{37}$$

By appropriately adjusting S_{cd} and S_{cq}, the system's energy storage function can converge rapidly, thus achieving rapid tracking of the relevant parameters.

The same law was applied to derive passive control laws for both positive and negative sequences. According to (37), we can derive the positive and negative sequence passive control laws for the BDFRG. They are represented by (38) and (39):

$$\begin{aligned} \begin{bmatrix} u_{cd}^+ \\ u_{cq}^+ \end{bmatrix} &= \begin{bmatrix} R_c & 0 \\ 0 & R_c \end{bmatrix} \begin{bmatrix} i_{cd}^{+*} \\ i_{cq}^{+*} \end{bmatrix} \\ &+ \begin{bmatrix} 0 & -\omega_c^+ L_m & 0 & -\omega_c^+ L_c \\ \omega_c^+ L_m & 0 & \omega_c^+ L_c & 0 \end{bmatrix} \begin{bmatrix} i_{pd}^{+*} \\ i_{pq}^{+*} \\ i_{cd}^{+*} \\ i_{cq}^{+*} \end{bmatrix} \\ &+ \begin{bmatrix} 2\omega_c^+ L_m i_{pq}^+ \\ -2L_m p i_{pq}^+ \end{bmatrix} - \begin{bmatrix} S_{cd}^+(i_{cd}^+ - i_{cd}^{+*}) \\ S_{cq}^+(i_{cq}^+ - i_{cq}^{+*}) \end{bmatrix} \end{aligned} \tag{38}$$

$$\begin{bmatrix} u_{cd}^{-} \\ u_{cq}^{-} \end{bmatrix} = \begin{bmatrix} R_c & 0 \\ 0 & R_c \end{bmatrix} \begin{bmatrix} i_{cd}^{-*} \\ i_{cq}^{-*} \end{bmatrix} + \begin{bmatrix} 0 & -\omega_c^{-} L_m & 0 & -\omega_c^{-} L_c \\ \omega_c^{-} L_m & 0 & \omega_c^{-} L_c & 0 \end{bmatrix} \begin{bmatrix} i_{pd}^{-*} \\ i_{pq}^{-*} \\ i_{cd}^{-*} \\ i_{cq}^{-*} \end{bmatrix} + \begin{bmatrix} 2\omega_c^{-} L_m i_{pq}^{-} \\ -2L_m p i_{pq}^{-} \end{bmatrix} - \begin{bmatrix} S_{cd}^{-}(i_{cd}^{-} - i_{cd}^{-*}) \\ S_{cq}^{-}(i_{cq}^{-} - i_{cq}^{-*}) \end{bmatrix} \tag{39}$$

When the BDFRG reaches a steady state $\boldsymbol{x}^* = \begin{bmatrix} i_{pd}^* & i_{pq}^* & i_{cd}^* & i_{cq}^* \end{bmatrix}^T$, the state variables do not change anymore. The stationary values of the positive and negative currents of the PW and CW sides are obtained as shown in (41) and (42). Due to:

$$\begin{cases} i_{pd} = i_{pd}^{+} + i_{pd}^{-} \\ i_{pq} = i_{pq}^{+} + i_{pq}^{-} \\ i_{cd} = i_{cd}^{+} + i_{cd}^{-} \\ i_{cq} = i_{cq}^{+} + i_{cq}^{-} \end{cases} \tag{40}$$

$$\begin{cases} i_{pq}^{+*} = \dfrac{2P^*}{3U_p^{+}} \\ i_{pd}^{+*} = \dfrac{2Q^*}{3U_p^{+}} \\ i_{cd}^{+*} = \dfrac{u_p^{+} - R_p i_{pq}^{+*} - \omega_p^{+} L_p i_{pd}^{+*}}{\omega_p^{+} L_m} \\ i_{cq}^{+*} = \dfrac{\omega_p^{+} L_p i_{pq}^{+*} - R_p i_{pd}^{+*}}{\omega_p^{+} L_m} \end{cases} \tag{41}$$

$$\begin{cases} i_{pq}^{-*} = \dfrac{2P^*}{3U_p^{-}} \\ i_{pd}^{-*} = \dfrac{2Q^*}{3U_p^{-}} \\ i_{cd}^{-*} = \dfrac{u_p^{-} - R_p i_{pq}^{-*} - \omega_p^{-} L_p i_{pd}^{-*}}{\omega_p^{-} L_m} \\ i_{cq}^{-*} = \dfrac{\omega_p^{-} L_p i_{pq}^{-*} - R_p i_{pd}^{-*}}{\omega_p^{-} L_m} \end{cases} \tag{42}$$

where, P^* is the reference value of active power, and Q^* is the reference value of reactive power. i_{pd}^{+*} and i_{pq}^{+*} are the given values of positive currents along the *d* and *q* axes, in the stator PW's positive sequence *d-q* rotating coordinate system. i_{cd}^{+*} and i_{cq}^{+*} are the given values of positive currents along the *d* and *q* axes, in the stator CW's positive sequence *d-q* rotating coordinate system. i_{pd}^{-*} and i_{pq}^{-*} are the given values of negative currents along the *d* and *q* axes, in the stator PW's negative sequence *d-q* rotating coordinate system. i_{cd}^{-*} and i_{cq}^{-*} are the given values of negative currents along the *d* and *q* axes, in the stator CW's negative sequence *d-q* rotating coordinate system.

By substituting (41) and (42) into (38) and (39), we can derive the passive control strategy for the BDFRG as follows:

$$\begin{cases} u_{cd} = u_{cd}^{+} + u_{cd}^{-} \\ \quad = R_c i_{cd}^{*} - \omega_c^{+} L_m i_{pq}^{+*} - \omega_c^{+} L_c i_{cq}^{+*} - \omega_c^{-} L_m i_{pq}^{-*} - \omega_c^{-} L_c i_{cq}^{-*} \\ \quad + 2\omega_c^{+} L_m i_{pq}^{+} + 2\omega_c^{-} L_m i_{pq}^{-} - S_{cd}(i_{cd} - i_{cd}^{*}) \\ u_{cq} = u_{cq}^{+} + u_{cq}^{-} \\ \quad = R_c i_{cq}^{*} + \omega_c^{+} L_m i_{pd}^{+*} + \omega_c^{+} L_c i_{cd}^{+*} + \omega_c^{-} L_m i_{pd}^{-*} + \omega_c^{-} L_c i_{cd}^{-*} \\ \quad - 2L_m p i_{pq} - S_{cq}(i_{cq} - i_{cq}^{*}) \end{cases} \tag{43}$$

IV. DESIGN OF PASSIVITY FEEDBACK CONTROLLER OF BDFRG UNDER UNBALANCED GRID VOLTAGES

In unbalanced grid voltage conditions, distortions occur in the stator currents, as well as second harmonic pulsations occur in the active and reactive power [29]. Therefore, it is necessary to separately adjust the positive and negative sequence components of the stator current to achieve our control objectives. Traditionally, passive control theory would employ a positive sequence passive state feedback controllers to control the positive sequence current and a negative sequence passive state feedback controllers for the negative sequence current. The extraction process of these sequence components introduces significant delays and errors into the signal, reducing the system's dynamic performance and stability.

To address this issue, this paper introduces a current control strategy that consists of a main controller and an auxiliary controller. The main controller directly controls the current within the positive sequence passive state feedback controllers, ensuring the system's output of active and reactive power direct current components, as detailed in (38) and (45). The auxiliary controller manages the negative sequence passive state feedback controllers, controlling only the negative sequence current [30].

However, since the feedback voltages of the CW side have only two parameters, it is not possible to control the above objectives at the same time [31]. Therefore, the passive state feedback controllers can separately achieve the following objectives.

Objective 1: Balance the three-phase currents of the PW and CW sides.

Objective 2: Maintain constant active power and suppress the second harmonic.

Objective 3: Maintain constant reactive power and suppress the second harmonic.

Objective 1:

In the negative sequence coordinate system, we can obtain the given values of negative currents in the stator.

$$\begin{cases} i_{pq}^{-*} = i_{pq1}^{-*} = 0 \\ i_{pd}^{-*} = i_{pd1}^{-*} = 0 \\ i_{cd}^{-*} = i_{cd1}^{-*} = 0 \\ i_{cq}^{-*} = i_{cq1}^{-*} = 0 \end{cases} \tag{44}$$

where, i_{pd1}^{-*} is the given value of i_{pd}^{-*} for achieving objective 1. i_{pq1}^{-*} is the given value of i_{pq}^{-*} for achieving objective 1. i_{cd1}^{-*} is the given value of i_{cd}^{-*} for achieving objective 1. i_{cq1}^{-*} is the given value of i_{cq}^{-*} for achieving objective 1.

By substituting into (39), we can obtain the negative voltages of the CW side:

$$\begin{bmatrix} u_{cd1}^{-} \\ u_{cq1}^{-} \end{bmatrix} = \begin{bmatrix} 2\omega_c^{-} L_m i_{pq}^{-} \\ -2L_m p i_{pq}^{-} \end{bmatrix} - \begin{bmatrix} S_{cd}^{-} i_{cd}^{-} \\ S_{cq}^{-} i_{cq}^{-} \end{bmatrix} \tag{45}$$

where, u_{cd1}^{-} is the negative sequence voltage along the *d*-axis of the CW side calculated for achieving objective 1. u_{cq1}^{-} is the negative sequence voltage along the *q*-axis of the CW side calculated for achieving objective 1.

The sum of (45) and (38) provides the feedback voltages of the CW side, which is obtained to achieve the objective 1.

$$\begin{aligned} \begin{bmatrix} u_{cd1} \\ u_{cq1} \end{bmatrix} &= \begin{bmatrix} u_{cd}^{+} + u_{cd1}^{-} \\ u_{cq}^{+} + u_{cq1}^{-} \end{bmatrix} \\ &= \begin{bmatrix} R_c & 0 \\ 0 & R_c \end{bmatrix} \begin{bmatrix} i_{cd}^{+*} \\ i_{cq}^{+*} \end{bmatrix} + \begin{bmatrix} 2\omega_c^{+} L_m i_{pq}^{+} + 2\omega_c^{-} L_m i_{pq}^{-} \\ -2L_m p i_{pq} \end{bmatrix} \\ &+ \begin{bmatrix} 0 & -\omega_c^{+} L_m & 0 & -\omega_c^{+} L_c \\ \omega_c^{+} L_m & 0 & \omega_c^{+} L_c & 0 \end{bmatrix} \begin{bmatrix} i_{pd}^{+*} \\ i_{pq}^{+*} \\ i_{cd}^{+*} \\ i_{cq}^{+*} \end{bmatrix} \\ &- \begin{bmatrix} S_{cd}(i_{cd} - i_{cd}^{+*}) \\ S_{cq}(i_{cq} - i_{cq}^{+*}) \end{bmatrix} \end{aligned} \tag{46}$$

where, u_{cd1} is the feedback voltage along the *d*-axis of the CW side calculated for achieving objective 1. u_{cq1} is the feedback voltage along the *q*-axis of the CW side calculated for achieving objective 1.

Objective 2:

To keep the active power constant, we can set the second harmonic cosine and sine pulsations of the active power to zero, meaning the given active power $P_{\cos} = P_{\sin} = 0$. In the negative sequence coordinate system, we can obtain the given values of negative currents in the stator.

$$\begin{cases} i_{pq}^{-*} = i_{pq2}^{-*} = \dfrac{U_{pd}^{+} i_{pd}^{-} + U_{pd}^{-} i_{pd}^{+} + U_{pq}^{-} i_{pq}^{+}}{-U_{pq}^{+}} \\ i_{pd}^{-*} = i_{pd2}^{-*} = \dfrac{-U_{pd}^{+} i_{pq}^{-} + U_{pd}^{-} i_{pq}^{+} - U_{pq}^{-} i_{pd}^{+}}{-U_{pq}^{+}} \\ i_{cd}^{-*} = i_{cd2}^{-*} = \dfrac{u_p^{-} - R_p i_{pq}^{-*} - \omega_p^{-} L_p i_{pd}^{-*}}{\omega_p^{-} L_m} \\ i_{cq}^{-*} = i_{cq2}^{-*} = \dfrac{\omega_p^{-} L_p i_{pq}^{-*} - R_p i_{pd}^{-*}}{\omega_p^{-} L_m} \end{cases} \tag{47}$$

where, i_{pd2}^{-*} is the given value of i_{cd}^{-*} for achieving objective 2. i_{pq2}^{-*} is the given value of i_{pq}^{-*} for achieving objective 2. i_{cd2}^{-*} is the given value of i_{cd}^{-*} for achieving objective 2. i_{cq2}^{-*} is the given value of i_{cq}^{-*} for achieving objective 2.

By substituting into (39), we can obtain the negative voltages of the CW side:

$$\begin{aligned} \begin{bmatrix} u_{cd2}^{-} \\ u_{cq2}^{-} \end{bmatrix} &= \begin{bmatrix} R_c & 0 \\ 0 & R_c \end{bmatrix} \begin{bmatrix} i_{cd2}^{-*} \\ i_{cq2}^{-*} \end{bmatrix} \\ &+ \begin{bmatrix} 0 & -\omega_c^{-} L_m & 0 & -\omega_c^{-} L_c \\ \omega_c^{-} L_m & 0 & \omega_c^{-} L_c & 0 \end{bmatrix} \begin{bmatrix} i_{pd2}^{-*} \\ i_{pq2}^{-*} \\ i_{cd2}^{-*} \\ i_{cq2}^{-*} \end{bmatrix} \\ &+ \begin{bmatrix} 2\omega_c^{-} L_m i_{pq}^{-} \\ -2L_m p i_{pq}^{-} \end{bmatrix} - \begin{bmatrix} S_{cd}^{-}(i_{cd}^{-} - i_{cd2}^{-*}) \\ S_{cq}^{-}(i_{cq}^{-} - i_{cq2}^{-*}) \end{bmatrix} \end{aligned} \tag{48}$$

where, u_{cd2}^{-} is the negative sequence voltage along the *d*-axis of the CW side calculated for achieving objective 2. u_{cq2}^{-} is the negative sequence voltage along the *q*-axis of the CW side calculated for achieving objective 2.

The sum of (48) and (38) provides the feedback voltages of the CW side, which is obtained to achieve the objective 2.

$$\begin{bmatrix} u_{cd2} \\ u_{cq2} \end{bmatrix} = \begin{bmatrix} u_{cd}^{+} + u_{cd2}^{-} \\ u_{cq}^{+} + u_{cq2}^{-} \end{bmatrix} = \begin{bmatrix} R_c & 0 \\ 0 & R_c \end{bmatrix} \begin{bmatrix} i_{cd}^{+*} + i_{cd2}^{-*} \\ i_{cq}^{+*} + i_{cq2}^{-*} \end{bmatrix} + \begin{bmatrix} 0 & -\omega_c^{+} L_m & 0 & -\omega_c^{+} L_c \\ \omega_c^{+} L_m & 0 & \omega_c^{+} L_c & 0 \end{bmatrix} \begin{bmatrix} i_{pd}^{+*} \\ i_{pq}^{+*} \\ i_{cd}^{+*} \\ i_{cq}^{+*} \end{bmatrix} + \begin{bmatrix} 0 & -\omega_c^{-} L_m & 0 & -\omega_c^{-} L_c \\ \omega_c^{-} L_m & 0 & \omega_c^{-} L_c & 0 \end{bmatrix} \begin{bmatrix} i_{pd2}^{-*} \\ i_{pq2}^{-*} \\ i_{cd2}^{-*} \\ i_{cq2}^{-*} \end{bmatrix} + \begin{bmatrix} 2\omega_c^{+} L_m i_{pq}^{+} + 2\omega_c^{-} L_m i_{pq}^{-} \\ -2L_m p i_{pq} \end{bmatrix} - \begin{bmatrix} S_{cd}(i_{cd} - (i_{cd}^{+*} + i_{cd2}^{-*})) \\ S_{cq}(i_{cq} - (i_{cq}^{+*} + i_{cq2}^{-*})) \end{bmatrix} \tag{49}$$

where, u_{cd2} is the feedback voltage along the *d*-axis of the CW side calculated for achieving objective 2. u_{cq2} is the feedback voltage along the *q*-axis of the CW side calculated for achieving objective 2.

Objective 3:

To keep the reactive power constant, we can set the second harmonic cosine and sine pulsations of the reactive power to zero, meaning the given reactive power $Q_{\cos} = Q_{\sin} = 0$. In the negative sequence coordinate system, we can obtain the given values of negative currents in the stator.

$$\begin{cases} i_{pq}^{-*} = i_{pq3}^{-*} = \dfrac{-U_{pd}^{+} i_{pd}^{-} - U_{pd}^{-} i_{pd}^{+} - U_{pq}^{-} i_{pq}^{+}}{U_{pq}^{+}} \\ i_{pd}^{-*} = i_{pd3}^{-*} = \dfrac{U_{pd}^{+} i_{pq}^{-} + U_{pd}^{-} i_{pq}^{+} - U_{pq}^{-} i_{pd}^{+}}{U_{pq}^{+}} \\ i_{cd}^{-*} = i_{cd3}^{-*} = \dfrac{u_p^{-} - R_p i_{pq}^{-*} - \omega_p^{-} L_p i_{pd}^{-*}}{\omega_p^{-} L_m} \\ i_{cq}^{-*} = i_{cq3}^{-*} = \dfrac{\omega_p^{-} L_p i_{pq}^{-*} - R_p i_{pd}^{-*}}{\omega_p^{-} L_m} \end{cases} \tag{50}$$

where, i_{pd3}^{-*} is the given value of i_{cd}^{-*} for achieving objective 3. i_{pq3}^{-*} is the given value of i_{pq}^{-*} for achieving objective 3. i_{cd3}^{-*} is the given value of i_{cd}^{-*} for achieving objective 3. i_{cq3}^{-*} is the given value of i_{cq}^{-*} for achieving objective 3.

By substituting into (39), we can obtain the negative voltages of the CW side:

$$\begin{bmatrix} u_{cd3}^{-} \\ u_{cq3}^{-} \end{bmatrix} = \begin{bmatrix} R_c & 0 \\ 0 & R_c \end{bmatrix} \begin{bmatrix} i_{cd3}^{-*} \\ i_{cq3}^{-*} \end{bmatrix} + \begin{bmatrix} 0 & -\omega_c^{-} L_m & 0 & -\omega_c^{-} L_c \\ \omega_c^{-} L_m & 0 & \omega_c^{-} L_c & 0 \end{bmatrix} \begin{bmatrix} i_{pd3}^{-*} \\ i_{pq3}^{-*} \\ i_{cd3}^{-*} \\ i_{cq3}^{-*} \end{bmatrix} + \begin{bmatrix} 2\omega_c^{-} L_m i_{pq}^{-} \\ -2L_m p i_{pq}^{-} \end{bmatrix} - \begin{bmatrix} S_{cd}^{-}(i_{cd}^{-} - i_{cd3}^{-*}) \\ S_{cq}^{-}(i_{cq}^{-} - i_{cq3}^{-*}) \end{bmatrix} \tag{51}$$

where, u_{cd3}^{-} is the negative sequence voltage along the *d*-axis of the CW side calculated for achieving objective 3. u_{cq3}^{-} is the negative sequence voltage along the *q*-axis of the CW side calculated for achieving objective 3.

The sum of (51) and (38) provides the feedback voltages of the CW side, which is obtained to achieve the objective 3.

$$\begin{bmatrix} u_{cd3} \\ u_{cq3} \end{bmatrix} = \begin{bmatrix} u_{cd}^{+} + u_{cd3}^{-} \\ u_{cq}^{+} + u_{cq3}^{-} \end{bmatrix} = \begin{bmatrix} R_c & 0 \\ 0 & R_c \end{bmatrix} \begin{bmatrix} i_{cd}^{+*} + i_{cd3}^{-*} \\ i_{cq}^{+*} + i_{cq3}^{-*} \end{bmatrix} + \begin{bmatrix} 0 & -\omega_c^{+} L_m & 0 & -\omega_c^{+} L_c \\ \omega_c^{+} L_m & 0 & \omega_c^{+} L_c & 0 \end{bmatrix} \begin{bmatrix} i_{pd}^{+*} \\ i_{pq}^{+*} \\ i_{cd}^{+*} \\ i_{cq}^{+*} \end{bmatrix} + \begin{bmatrix} 0 & -\omega_c^{-} L_m & 0 & -\omega_c^{-} L_c \\ \omega_c^{-} L_m & 0 & \omega_c^{-} L_c & 0 \end{bmatrix} \begin{bmatrix} i_{pd3}^{-*} \\ i_{pq3}^{-*} \\ i_{cd3}^{-*} \\ i_{cq3}^{-*} \end{bmatrix} + \begin{bmatrix} 2\omega_c^{+} L_m i_{pq}^{+} + 2\omega_c^{-} L_m i_{pq}^{-} \\ -2L_m p i_{pq} \end{bmatrix} - \begin{bmatrix} S_{cd}(i_{cd} - (i_{cd}^{+*} + i_{cd3}^{-*})) \\ S_{cq}(i_{cq} - (i_{cq}^{+*} + i_{cq3}^{-*})) \end{bmatrix} \tag{52}$$

where, u_{cd3} is the feedback voltage along the *d*-axis of the CW side calculated for achieving objective 3. u_{cq3} is the feedback voltage along the *q*-axis of the CW side calculated for achieving objective 3.

The resulting negative currents in the stator can be used to calculate the negative voltages of the CW side by substituting into the passive control laws. By feeding back the negative voltages of the CW side into the system, it is possible to effectively suppress the distortions in the stator currents and the second harmonic pulsations in active and reactive power under unbalanced grid voltages, thereby achieving the corresponding control objectives.

V. EXPERIMENTAL RESULTS ANALYSIS

A. SIMULATION ANALYSIS

In unbalanced grid voltage conditions, the multi-objective control structure diagram for the BDFRG is illustrated in Fig. 4.

To confirm the efficiency of the control strategy adopted in the BDFRG operational system under unbalanced grid voltages, a passive control simulation model for the BDFRG was developed using the MATLAB/Simulink platform. The relevant parameters are given in Table II.

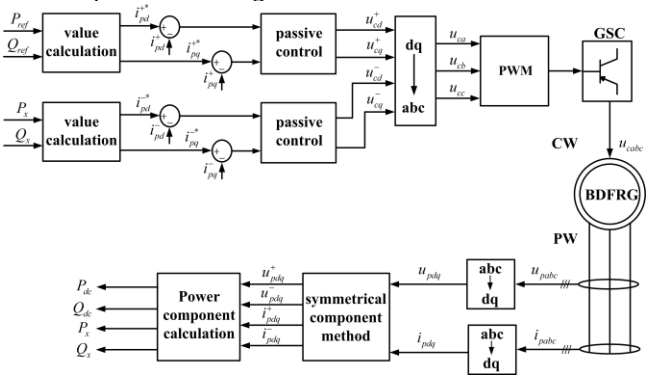

FIGURE 4. Multi-objective control structure diagram for the BDFRG under unbalanced grid voltages

TABLE II
BDFRG RELATED PARAMETERS

Parameter	Value
Pole pairs of the PW p_p	3
Pole pairs of the CW p_c	1
Resistance of the PW R_p (Ω)	0.1662
Resistance of the CW R_c (Ω)	0.1882
Self-inductance of the PW L_p (H)	0.01737
Self-inductance of the CW L_c (H)	0.02351
Mutual inductance between the PW and CW L_m (H)	0.01813

In the simulation of the BDFRG, the speed of the rotor is given to 450 r/min, with active power given to 5 kW and reactive power given to -5 kvar. The stator voltage is in an unbalanced state at 3 seconds and returns to normal at 4.5 seconds. For different control objectives, the control effects before and after adding the negative voltage control to the system are compared in the simulation.

The waveform of grid voltage under unbalanced grid voltages in the simulation is shown in Fig. 5.

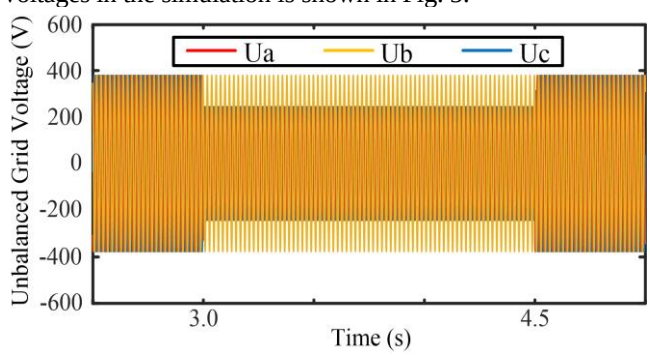

FIGURE 5. The waveform of unbalanced grid voltages

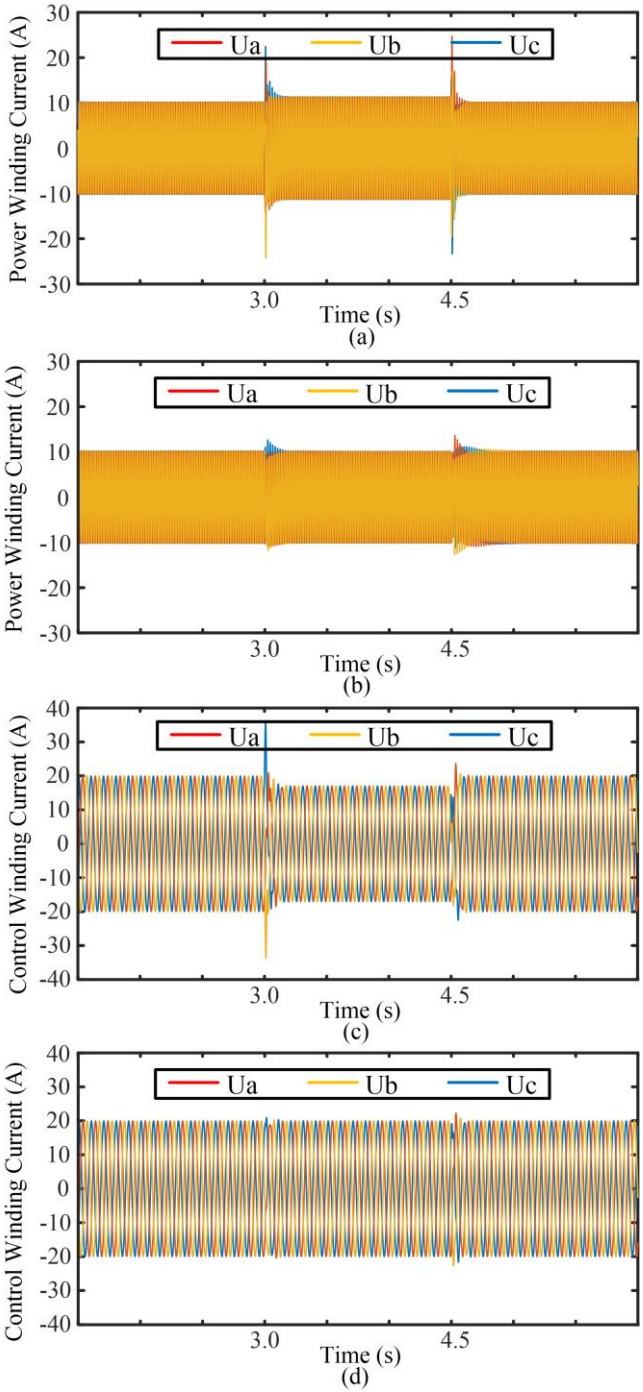

FIGURE 6. The waveform of currents. (a) The PW side current before adding the negative voltage control. (b) The PW side current after adding the negative voltage control. (c) The CW side current before adding the negative voltage control. (d) The CW side current after adding the negative voltage control

For the problem of distortions in the stator currents as mentioned in objective 1, a simulation study of the passive control for the BDFRG under unbalanced grid voltages was conducted. The control effects before and after adding the negative voltages u_{cdq1}^{-} to the control system are compared. In Fig. 6, (a) and (c) represent the waveforms of the PW and CW sides currents before adding the negative voltage control,

while (b) and (d) represent the waveforms of the PW and CW sides currents after adding the negative voltage control. From the simulation waveforms, we can observe that the PW and CW sides currents exhibit distortions under unbalanced grid voltages. After adding the negative voltage control, the distortions in the stator current waveforms are suppressed, and they tend toward sinusoidal. Furthermore, the amplitudes of the modified current waveforms remain the same as before, without significant changes.

For the problem of second harmonic pulsations in the active power as mentioned in objective 2, a simulation study on passive control for BDFRG under unbalanced grid voltages was conducted. The control effects before and after adding the negative voltages u_{cdq2}^{-} to the control system are compared. In Fig. 7, (a) represents the waveform of active power before adding the negative voltage control, while (b) represents the waveform of active power after adding the negative voltage control. From the simulation waveforms, we can observe that under unbalanced grid voltages, the active power exhibits second harmonic pulsation. After adding the negative voltage control, the second harmonic pulsations in active power are efficiently reduced, and the active power can track the given active power well.

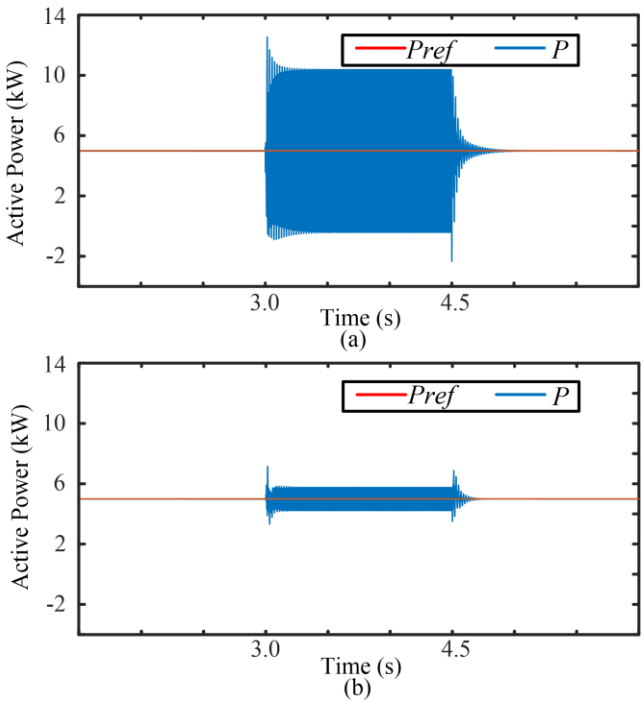

FIGURE 7. The waveform of active power. (a) Before adding the negative voltage control. (b) After adding the negative voltage control.

For the problem of second harmonic pulsations in the reactive power as mentioned in objective 3, a simulation study on passive control for BDFRG under unbalanced grid voltages was conducted. The control effects before and after adding the negative voltages u_{cdq3}^{-} to the control system are compared. In Fig. 8, (a) represents the waveform of reactive power before adding the negative voltage control, while (b) represents the waveform of reactive power after adding the negative voltage control. From the simulation waveforms, we can observe that under unbalanced grid voltages, the reactive power exhibits second harmonic pulsation. After adding the negative voltage control, the second harmonic pulsations in reactive power are efficiently reduced, and the reactive power can track the given reactive power well.

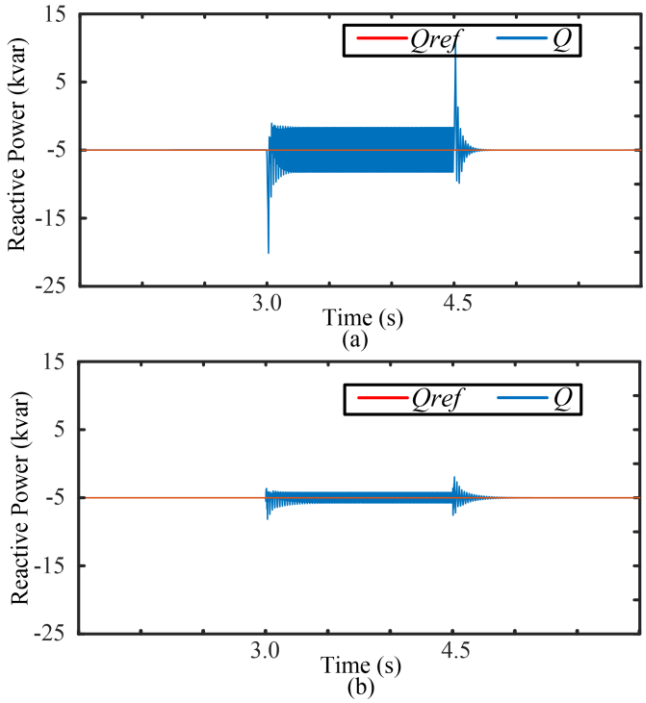

FIGURE 8. The waveform of reactive power. (a) Before adding the negative voltage control. (b) After adding the negative voltage control.

B. EXPERIMENTAL VALIDATION

A hardware-in-the-loop experimental platform, as illustrated in Fig. 9, was constructed to further demonstrate the effectiveness and reliability of the passive control for the BDFRG under unbalanced grid voltages.

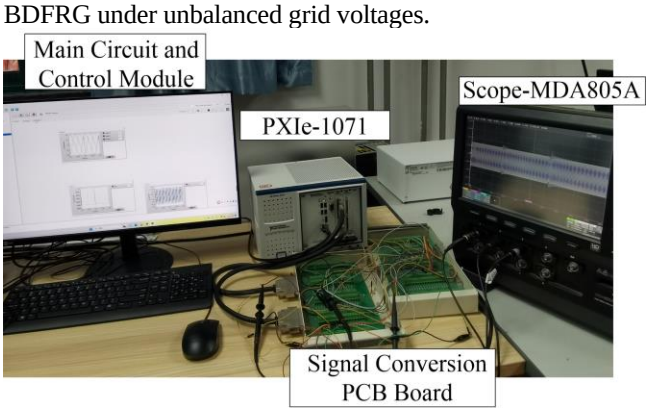

FIGURE 9. Hardware-in-the-loop experimental platform

This platform utilizes the NI PXIe-1071 as the controller and the experimental main circuit construction carrier. The control chip is Xilinx K7-160T FPGA, and the oscilloscope is the Lecroy MDA805A. The BDFRG main circuit is constructed in the Start Sim software, and the Start Sim HIL software is used to combine the main circuit with the control circuit.

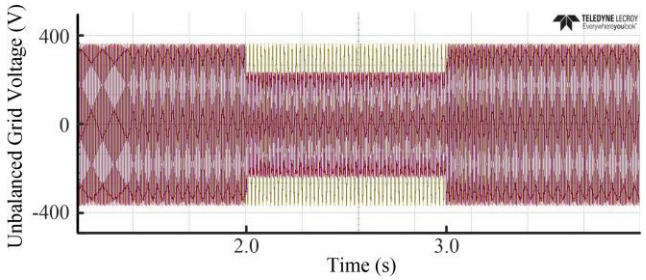

FIGURE 10. **The experimental voltage waveform of unbalanced grid voltages**

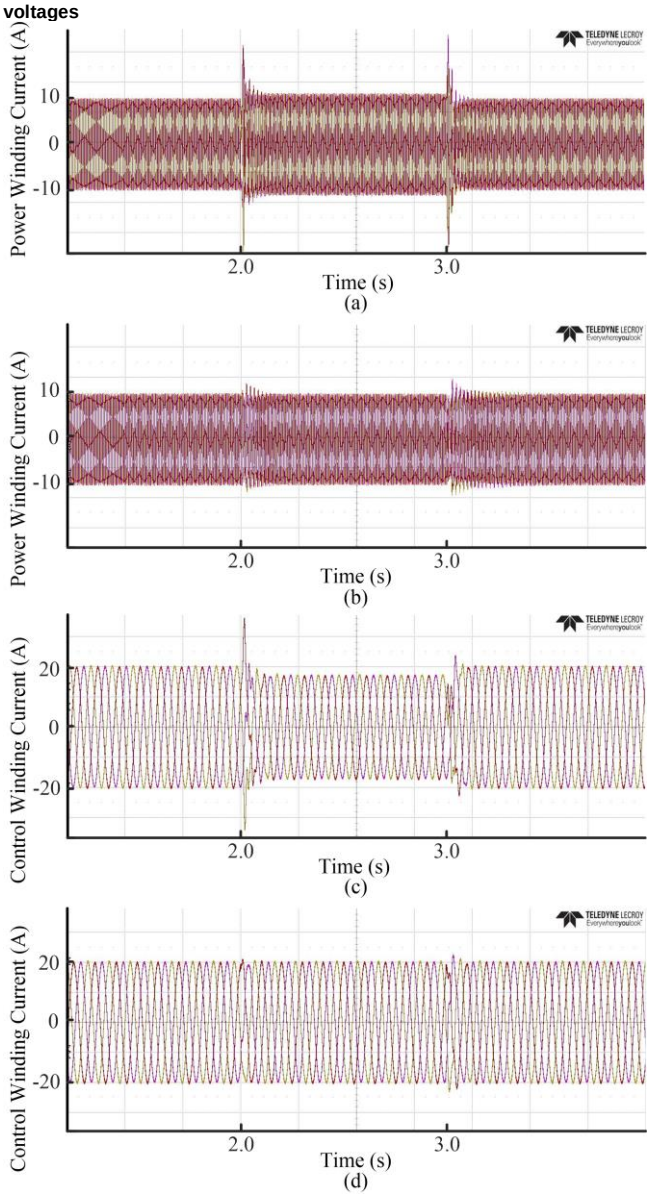

FIGURE 11. **The experimental waveform of currents. (a) The PW side current before adding the negative voltage control. (b) The PW side current after adding the negative voltage control. (c) The CW side current before adding the negative voltage control. (d) The CW side current after adding the negative voltage control.**

On the above platform, experiment with the dynamic changes of PW and CW sides currents, as well as active and reactive power. Observe the variations before and after adding the negative voltage control. Study the control effect of different objectives under unbalanced grid voltages.

The BDFRG speed is set to 450 r/min in the experiment, with an active power setpoint of 5 kW and a reactive power setpoint of -5 kvar. At 2 seconds, the stator voltage is in an unbalanced state, returning to normal at 3 seconds. The control effects before and after adding the negative voltage control are compared in the experiment. The experimental voltage waveform of unbalanced grid voltages is displayed in Fig. 10.

To address the problem of distortions in the stator currents as mentioned in objective 1, we compare the control effects before and after adding the negative voltage control. From the results, we can observe that the PW and CW sides currents exhibit distortions when the grid is in an unbalanced state as illustrated in Fig. 11. After adding the negative voltage control, the distortions in the stator currents are suppressed.

To address the problem of second harmonic pulsations in the active power as mentioned in objective 2, we compare the control effects before and after adding the negative voltage control. From the results, we can observe that the active power exhibits second harmonic pulsations when the grid is in an unbalanced state as illustrated in Fig. 12. After adding the negative voltage control, the second harmonic pulsations in the active power are efficiently reduced, and the active power can follow the given active power well.

To address the problem of second harmonic pulsations in the reactive power as mentioned in objective 3, we compare the control effects before and after adding the negative voltage control. From the results, we can observe that the reactive power exhibits second harmonic pulsations when the grid is in an unbalanced state as illustrated in Fig. 13. After adding the negative voltage control, the second harmonic pulsations in the reactive power are efficiently reduced, and the reactive power can follow the given reactive power well.

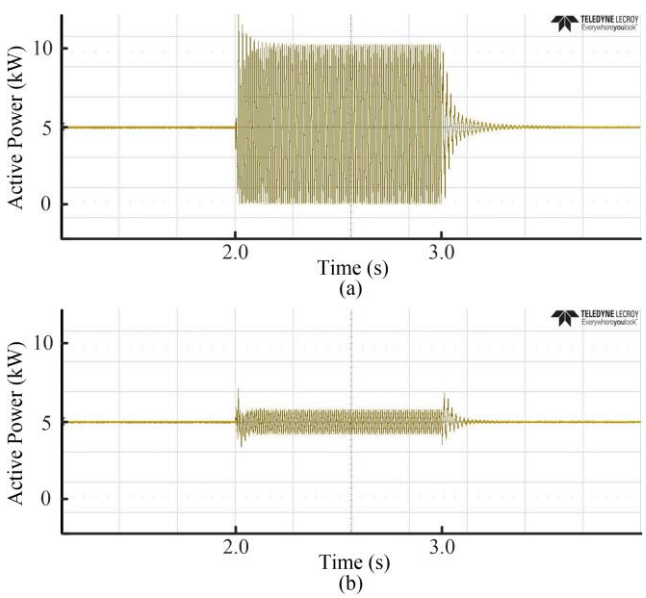

FIGURE 12. **The experimental waveform of active power. (a) Before adding the negative voltage control. (b) After adding the negative voltage control.**

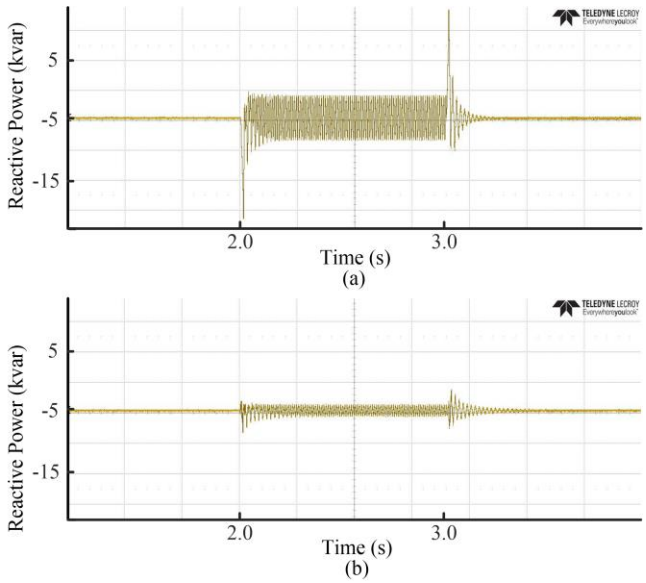

FIGURE 13. The experimental waveform of reactive power. (a) Before adding the negative voltage control. (b) After adding the negative voltage control.

We performed Fast Fourier Transform (FFT) analysis on the output current of the generator's stator PW side under unbalanced grid conditions. The analysis showed that the total harmonic distortion (THD) was 1.71%, which is significantly below the standards required for grid interconnection, demonstrating the effectiveness of passive control in enhancing power quality. The FFT analysis of the generator stator PW side current waveform is shown in Fig. 14.

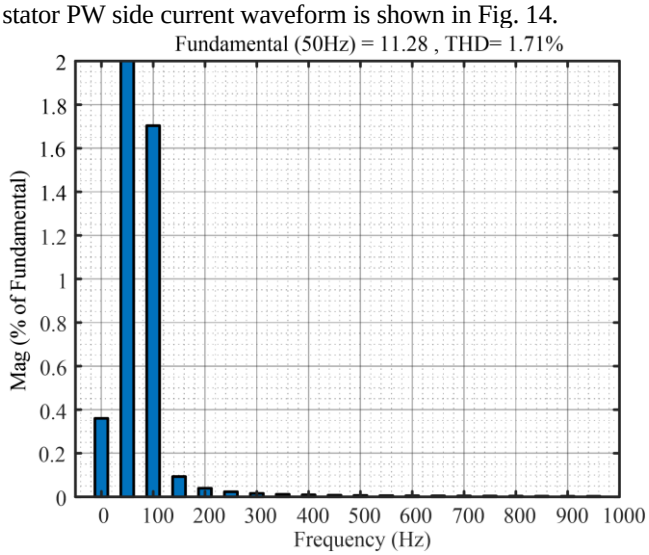

FIGURE 14. Analysis of THD in Power Winding Current

VI. CONCLUSION

Based on the symmetrical component method, the positive and negative sequence theoretical model of BDFRG under unbalanced grid voltages was derived. According to the EL model and the passivity theory, we not only analyzed the passivity characteristics of BDFRG from the energy, but also proposed the passive control strategy. The reference values of the negative sequence currents of the PW and CW sides were calculated by different control objectives, and the passive feedback controllers can be designed by substituting them into the passive control strategy proposed. Simulation and experimental results demonstrated that the designed passive feedback controllers could effectively suppress distortions in the stator currents and second harmonic pulsations in the active and reactive power according to different objectives, which validated the correctness of the derived model and the effectiveness of the control strategy.

REFERENCES

[1] Y. Liu, M. G. Hussien, W. Xu, S. Shao, and E. M. Rashad, "Recent Advances of Control Technologies for Brushless Doubly-Fed Generators," *IEEE Access*, vol. 9, pp. 123324–123347, 2021, doi: 10.1109/ACCESS.2021.3110373.

[2] Y. Jiang, J. Zhang, and T. Li, "A Segmented Brushless Doubly Fed Generator for Wind Power Applications," *IEEE Transactions on Magnetics*, vol. 54, no. 3, pp. 1–4, Mar. 2018, doi: 10.1109/TMAG.2017.2762827.

[3] J. Su, Y. Chen, and Y. Kang, "A Comprehensive Study on Model Simplification and Parameter Estimation of Brushless Doubly Fed Standalone Generation System," *IEEE Transactions on Industrial Electronics*, vol. 71, no. 4, pp. 3405–3417, Apr. 2024, doi: 10.1109/TIE.2023.3273271.

[4] M.-F. Hsieh, Y.-H. Chang, and D. G. Dorrell, "Design and Analysis of Brushless Doubly Fed Reluctance Machine for Renewable Energy Applications," *IEEE Transactions on Magnetics*, vol. 52, no. 7, pp. 1–5, Jul. 2016, doi: 10.1109/TMAG.2016.2537140.

[5] O. I. Olubamiwa, T. Hutton, and N. Gule, "Brushless Doubly Fed Machine Design Evaluation With Power Factor Considerations," *IEEE Transactions on Industry Applications*, vol. 59, no. 2, pp. 1457–1468, Mar. 2023, doi: 10.1109/TIA.2022.3217750.

[6] K. Kiran, S. Das, and D. Singh, "Model predictive field oriented speed control of brushless doubly-fed reluctance motor drive," in *2018 International Conference on Power, Instrumentation, Control and Computing (PICC)*, Jan. 2018, pp. 1–6. doi: 10.1109/PICC.2018.8384760.

[7] E. F. Yassin, H. M. Yassin, A. Hemeida, and M. M. Hallouda, "Real Time Simulation of Brushless Doubly Fed Reluctance Generator Driven Wind Turbine Considering Iron Saturation," *IEEE Access*, vol. 10, pp. 9925–9934, 2022, doi: 10.1109/ACCESS.2022.3144600.

[8] E. F. Yassin, H. M. Yassin, and M. M. Hallouda, "Control Strategies for Brushless Doubly Fed Reluctance Generator in WECS: Review," in *2021 IEEE International Conference in Power Engineering Application (ICPEA)*, Mar. 2021, pp. 79–84. doi: 10.1109/ICPEA51500.2021.9417838.

[9] T. Taluo, L. Ristić, and M. Jovanović, "Steady-State Analysis of DFIGs and BDFRGs," in *2022 7th International Conference on Environment Friendly Energies and Applications (EFEA)*, Dec. 2022, pp. 1–6. doi: 10.1109/EFEA56675.2022.10063805.

[10] X. Yan and M. Cheng, "Backstepping-Based Direct Power Control for Dual-Cage Rotor Brushless Doubly Fed Induction Generator," *IEEE Transactions on Power Electronics*, vol. 38, no. 2, pp. 2668–2680, Feb. 2023, doi: 10.1109/TPEL.2022.3214331.

[11] W. Xu, M. G. Hussien, Y. Liu, Md. R. Islam, and S. M. Allam, "Sensorless Voltage Control Schemes for Brushless Doubly-Fed Induction Generators in Stand-Alone and Grid-Connected Applications," *IEEE Transactions on Energy Conversion*, vol. 35, no. 4, pp. 1781–1795, Dec. 2020, doi: 10.1109/TEC.2020.2999629.

[12] Y. Zeng, M. Cheng, X. Wei, and G. Zhang, "Grid-Connected and Standalone Control for Dual-Stator Brushless Doubly Fed Induction Generator," *IEEE Transactions on Industrial Electronics*, vol. 68, no. 10, pp. 9196–9206, Oct. 2021, doi: 10.1109/TIE.2020.3028824.

[13] H. Lu, D. Zhang, C. Qu, and Z. Zhang, "Modeling and Analysis of Brushless Doubly-Fed Induction Generators with Non-Ideal Grids," in *2022 5th International Conference on Energy, Electrical and Power Engineering (CEEPE)*, Apr. 2022, pp. 412–419. doi: 10.1109/CEEPE55110.2022.9783125.

[14] S. Hu, G. Zhu, and Y. Kang, "Modeling and Coordinated Control Design for Brushless Doubly-Fed Induction Generator-Based Wind

Turbine to Withstand Grid Voltage Unbalance," *IEEE Access*, vol. 9, pp. 63331–63344, 2021, doi: 10.1109/ACCESS.2021.3074528.

[15] Y. Liu, W. Xu, D. Hu, and F. Blaabjerg, "Harmonic Voltage and Current Elimination of Stand-Alone Brushless Doubly-Fed Induction Generator with Nonlinear Loads for Ship Shaft Power Generation Applications," in *2018 IEEE Energy Conversion Congress and Exposition (ECCE)*, Sep. 2018, pp. 7349–7355. doi: 10.1109/ECCE.2018.8558337.

[16] O. M. Elbabo Mohammed, Y. Liu, W. Xu, and Md. R. Islam, "An Enhanced Control Strategy for Standalone Brushless Doubly Fed Induction Generator Under Unbalanced Load Using Reactive Power Loop," in *2022 IEEE IAS Global Conference on Emerging Technologies (GlobConET)*, May 2022, pp. 492–496. doi: 10.1109/GlobConET53749.2022.9872349.

[17] X. Yang, J. Bai, Y. Qin, and J. Zhao, "Direct power control of a brushless doubly-fed induction generator under an unbalanced power grid," in *2023 2nd Asia Conference on Electrical, Power and Computer Engineering (EPCE)*, Apr. 2023, pp. 99–109. doi: 10.1109/EPCE58798.2023.00026.

[18] J. Chen, W. Zhang, B. Chen, and Y. Ma, "Improved Vector Control of Brushless Doubly Fed Induction Generator under Unbalanced Grid Conditions for Offshore Wind Power Generation," *IEEE Transactions on Energy Conversion*, vol. 31, no. 1, pp. 293–302, Mar. 2016, doi: 10.1109/TEC.2015.2479859.

[19] M. Cheng, Y. Jiang, P. Han, and Q. Wang, "Unbalanced and Low-Order Harmonic Voltage Mitigation of Stand-Alone Dual-Stator Brushless Doubly Fed Induction Wind Generator," *IEEE Transactions on Industrial Electronics*, vol. 65, no. 11, pp. 9135–9146, Nov. 2018, doi: 10.1109/TIE.2017.2779422.

[20] X. Lv, Z. Kang, and Y.-C. Mei, "Double dq control strategy of DFIG based on passivity theory under unbalanced grid voltage," in *Proceedings of the 32nd Chinese Control Conference*, Jul. 2013, pp. 8851–8856.

[21] J. Hu, Y. He, L. Xu, and B. W. Williams, "Improved Control of DFIG Systems During Network Unbalance Using PI–R Current Regulators," IEEE Trans. Ind. Electron., vol. 56, no. 2, pp. 439–451, Feb. 2009, doi: 10.1109/TIE.2008.2006952.

[22] M. Kenan Döşoğlu, "A new approach for low voltage ride through capability in DFIG based wind farm," International Journal of Electrical Power & Energy Systems, vol. 83, pp. 251–258, Dec. 2016, doi: 10.1016/j.ijepes.2016.04.027.

XIAOLIANG YANG was born in Hebei, China, in 1980. He received his B.S. and M.S. degrees in electrical engineering in 2003 and 2009 from Zhengzhou University of Light Industry, Zhengzhou, China, and the Ph.D. degree in control science and engineering in 2021 from Hunan University, Changsha, China. He is currently an associate professor in Electrical Engineering with Zhengzhou University of Light Industry. His current research interests include wind power turbine control and motor control.

YIXUAN QIN was born in Henan, China. She received the B.S. degree in electrical engineering from Taiyuan University of Science and Technology, Taiyuan, China, in 2022. She is currently working toward the M.S. degree in electrical engineering, Zhengzhou University of Light Industry, Zhengzhou, China. Her research interests include brushless doubly-fed reluctance generator grid-connected operation control.

[23] S. Xiao, G. Yang, H. Zhou, and H. Geng, "An LVRT Control Strategy Based on Flux Linkage Tracking for DFIG-Based WECS," IEEE Trans. Ind. Electron., vol. 60, no. 7, pp. 2820–2832, Jul. 2013, doi: 10.1109/TIE.2012.2205354.

[24] M. K. Döşoğlu, U. Güvenç, Y. Sönmez, and C. Yılmaz, "Enhancement of demagnetization control for low-voltage ride-through capability in DFIG-based wind farm," Electr Eng, vol. 100, no. 2, pp. 491–498, Jun. 2018, doi: 10.1007/s00202-017-0522-6.

[25] M. K. Döşoğlu, O. Özkaraca, and U. Güvenç, "Novel active–passive compensator–supercapacitor modeling for low-voltage ride-through capability in DFIG-based wind turbines," Electr Eng, vol. 101, no. 4, pp. 1119–1132, Dec. 2019, doi: 10.1007/s00202-019-00857-y.

[26] M. Moazen, R. Kazemzadeh, and M.-R. Azizian, "Mathematical modeling and analysis of brushless doubly fed reluctance generator under unbalanced grid voltage condition," *International Journal of Electrical Power & Energy Systems*, vol. 83, pp. 547–559, Dec. 2016, doi: 10.1016/j.ijepes.2016.04.050.

[27] L. Xu, M. Cheng, X. Wei, and Y. Zeng, "Control and Operation of Brushless Doubly-Fed Induction Generator under Unbalanced Network," in *2020 23rd International Conference on Electrical Machines and Systems (ICEMS)*, Nov. 2020, pp. 1184–1189. doi: 10.23919/ICEMS50442.2020.9291157.

[28] L. Xu, M. Cheng, X. Wei, X. Yan, and Y. Zeng, "Dual Synchronous Rotating Frame Current Control of Brushless Doubly Fed Induction Generator Under Unbalanced Network," *IEEE Transactions on Power Electronics*, vol. 36, no. 6, pp. 6712–6724, Jun. 2021, doi: 10.1109/TPEL.2020.3039537.

[29] Y. Zhang and J. Jiao, "Model Predictive Rotor Current Control for Doubly Fed Induction Generators under Unbalanced Grid Voltages," in *2018 IEEE International Power Electronics and Application Conference and Exposition (PEAC)*, Shenzhen: IEEE, Nov. 2018, pp. 1–5. doi: 10.1109/PEAC.2018.8590608.

[30] L. Xu, M. Cheng, X. Wei, and Y. Zeng, "Control and Operation of Brushless Doubly-Fed Induction Generator under Unbalanced Network," in 2020 23rd International Conference on Electrical Machines and Systems (ICEMS), Nov. 2020, pp. 1184–1189. doi: 10.23919/ICEMS50442.2020.9291157.

[31] W. Xu, O. M. Elbabo Mohammed, Y. Liu, and Md. R. Islam, "Negative Sequence Voltage Compensating for Unbalanced Standalone Brushless Doubly-Fed Induction Generator," *IEEE Transactions on Power Electronics*, vol. 35, no. 1, pp. 667–680, Jan. 2020, doi: 10.1109/TPEL.2019.2912820

JIAJUN BAI was born in Henan, China. He received the M.S. degree in electrical engineering from Zhengzhou University of Light Industry, Zhengzhou, China, in 2023. He is currently working in State Grid Xin Yuan Company Limited, Zhengzhou, China. He is engaged in the stable operation of pumped storage production business, ensuring the stable operation of the power grid to achieve power supply guarantee.

JIHAO ZHAN was born in Henan, China. He received the B.S. degree in electrical engineering and automation from Xinke College of Henan Institute of Science and Technology Xinxiang, China, in 2021. He is currently working toward the M.S degree in electrical engineering, Zhengzhou University of Light Industry, Zhengzhou, China. His research interests include parameter identification of permanent magnet synchronous motor.

YIHAO LI was born in Henan, China. He received the B.S. degree in electrical engineering from Zhengzhou University of Light Industry, Zhengzhou, China, in 2021. He is currently working toward the M.S. degree in electrical engineering, Zhengzhou University of Light Industry, Zhengzhou, China. His research interests include finite control set model predictive control for virtual synchronous generator.

SUYA HAO was born in Shandong, China. She received the B.S. degree in electrical engineering and automation from Ludong University, Yantai, China, in 2023. She is currently working toward the M.S. degree in electrical engineering, Zhengzhou University of Light Industry, Zhengzhou, China. Her research interests include brushless double-fed induction generator control.